RSC Advances

PAPER

Cite this: *RSC Adv.*, 2014, **4**, 30241

Hydrogenation mechanism of carbon dioxide and carbon monoxide on Ru(0001) surface: a density functional theory study†

Shi-Tong Zhang, Hong Yan,* Min Wei,* David G. Evans and Xue Duan

Received 25th February 2014
Accepted 20th June 2014

DOI: 10.1039/c4ra01655f

www.rsc.org/advances

Catalytic hydrogenation of CO_2 or CO to chemicals/fuels is of great significance in chemical engineering and the energy industry. In this work, density functional theory (DFT) calculations were carried out to investigate the hydrogenation of CO_2 and CO on Ru(0001) surface to shed light on the understanding of the reaction mechanism, searching new catalysts and improving reaction efficiency. The adsorption of intermediate species (*e.g.*, COOH, CHO and CH), reaction mechanisms, reaction selectivity and kinetics were systematically investigated. The results showed that on Ru(0001) surface, CO_2 hydrogenation starts with the formation of an HCOO intermediate and produces adsorbed CHO and O species, followed by CHO dissociation to CH and O; while CO hydrogenation occurs *via* either a COH or CHO intermediate. Both the hydrogenation processes produce active C and CH species, which subsequently undergoes hydrogenation to CH_4 or a carbon chain growth reaction. The kinetics study indicates that product selectivity (methane or liquid hydrocarbons) is determined by the competition between the two most favorable reactions: CH + H and CH + CH. Methane is the predominant product with a high H_2 fraction at normal reaction pressure; while liquid hydrocarbons are mainly produced with a large CO_2/CO fraction at a relatively high pressure.

1. Introduction

Our current civilization depends mostly on energy produced by burning fossil fuels, which releases a large amount of carbon dioxide and carbon monoxide into the atmosphere. In the past decade, the catalytic hydrogenation of CO_2 and CO to useful chemicals (*e.g.*, methane and alcohol) has attracted increasing interest for effectively mitigating CO_2 and CO buildup and circularly utilizing the carbon resource.[1–4] For these hydrogenation reactions, noble metal-based catalysts (*e.g.*, Ru, Rh and Pd) have been widely accepted as the most efficient catalysts because of their high activity, low reaction temperature and product selectivity.[5–9] Although considerable investigations on CO_2 and CO hydrogenation have been carried out based on experimental and theoretical studies,[10–15] detailed reaction mechanisms and key intermediates of these processes are still under debate.[8,16–24] From the viewpoint of catalyst design and recycling of carbon, a fundamental understanding and theoretical insights into the hydrogenation process and mechanism of CO_2/CO on the noble-metal surface are of crucial significance and remain a challenging task.

For the CO_2 hydrogenation process, the main question is whether the reaction starts from C–O bond breaking or hydrogen association followed by C–O bond breaking. Mostly, it is assumed that CO_2 initially transforms to carbonyl (CO) *via* the reverse water gas shift (RWGS, $CO_2 + H_2 \rightarrow CO + H_2O$) with the formation of a formate (COOH) intermediate.[16,17,22] However, Behm *et al.* recently proposed that the adsorbed CO_2 molecule first dissociates to CO and O ($CO_2 \rightarrow CO + O$) during study of CO_2/CO methanation on a Ru catalyst.[21] Some other researchers have suggested that H prefers to first bind at the C-end of the CO_2 molecule to form an HCOO intermediate.[24] For CO hydrogenation, the reaction mechanism is similarly controversial. It is still not clear whether the initial step of the hydrogenation process is hydrogen association with CO to produce a CHO/COH intermediate or the direct dissociation of CO to carbon and oxygen. The experimental studies of Mitchell *et al.* and theoretical results of Inderwildi *et al.* demonstrated the formation of a CHO intermediate from co-adsorbed CO and H on the Ru surface.[25,26] However, Andersson *et al.* proposed that CO dissociation may proceed *via* a COH intermediate.[19] Earlier studies reported that CO directly dissociates in the initial step ($CO \rightarrow C + O$), resulting in an active carbon species, which undergoes stepwise hydrogenation to CH, CH_2, CH_3, and finally to CH_4.[27–29] This viewpoint was again reported in a recent study by Shetty *et al.* on the Ru(1121) surface.[30]

As an important supplementary technique to experimental investigations, theoretical methods can provide deeper insight

---

State Key Laboratory of Chemical Resource Engineering, Beijing University of Chemical Technology, Beijing 100029, China. E-mail: yanhong@mail.buct.edu.cn; weimin@mail.buct.edu.cn; Fax: +86-10-64425385; Tel: +86-10-64412131

† Electronic supplementary information (ESI) available: The detailed reaction energy and activation barrier of each elementary step (Fig. S1–S16) and kinetic analysis theory. See DOI: 10.1039/c4ra01655f

into reaction mechanisms and key factors that control the reactivity and selectivity by systematically investigating the reaction. However, most of the computational studies related to CO_2 and CO hydrogenations were focused on parts of the hydrogenation process such as methanation from C, hydrogen-assisted CO dissociation and C–C coupling reactions;[26,30–34] information regarding the entire reaction process of CO_2/CO hydrogenation as well as its selectivity is relatively rare. Therefore, a systematically theoretical investigation on CO_2/CO hydrogenation in the presence of noble-metal catalysts is highly desirable for understanding the reaction mechanism, designing/searching new catalysts and improving reaction efficiency.

In this study, we employed density functional theory (DFT) to investigate CO_2 and CO hydrogenation on the flat Ru(0001) surface, including the adsorption of the intermediate species, identification of the reaction mechanism, and unveiling the reaction selectivity and kinetics. The results show that the adsorbed CO_2 initially prefers to dissociate to CHO and O *via* an HCOO intermediate, and CHO tends to dissociate to active CH and O species. The CO hydrogenation process occurs *via* either a COH or CHO intermediate and then produces active C and CH species, which subsequently undergoes stepwise hydrogenation to CH, CH_2, CH_3 and CH_4 or generates C–C coupling products. The selectivity of the final product (methane or liquid hydrocarbons) is controlled by the competition between the CH + H and CH + CH reactions, which are the most favorable pathways for carbon hydrogenation and C–C coupling reactions, respectively. This work provides a fundamental understanding for the reaction processes of CO_2/CO hydrogenation on the Ru(0001) surface, which provides helpful instructions in the pursuit of the effective utilization of noble metal catalysts and CO_2/CO recycling.

2. Computational method and details

First-principle calculations within the DFT framework were performed with the DMol^3 code in the Materials Studio 5.5 software package.[35–37] The exchange-correlation potential was described by the Perdew-Wang 1991 (PW91) generalized gradient approach (GGA).[38] The atomic orbitals were represented by double numerical basis sets plus polarization function (DNP). The core electrons for metals were treated by effective core potentials (ECP). SCF converged criterion was within 1.0×10^{-5} hartree per atom and the converge criterion of structure optimization was 2.0×10^{-5} hartree per bohr. Brillouin zone sampling was performed using a Monkhorst-Pack grid.

The Ru(0001) surface was represented as a four-layered slab with $p(2 \times 2)$ supercell, and only the bottom atoms of the slab were constrained to their crystal lattice positions. The neighboring slabs were separated in a direction perpendicular to the surface by a vacuum region of 12 Å. The first Brillouin zone of the $p(2 \times 2)$ supercell was sampled with a $5 \times 5 \times 1$ *k*-point grid. Transition state (TS) searches were performed at the same theoretical level with the complete LST/QST method.[20] This method begins by performing a linear synchronous transit (LST)/optimization calculation. The transition state (TS) approximation obtained was used to perform a quadratic synchronous transit (QST) maximization. Based on the maximization point, another constrained minimization was performed, and the cycle was repeated until a stationary point was located. The LST/QST results were subsequently optimized to find the true stable point with a unique negative frequency. The energies of the initial states, transition states and final states were corrected by zero point energies (ZPE). The adsorption energies (E_{ads}) of the species adsorbed on the Ru(0001) surface were calculated from the energy difference between the optimized surface containing the adsorbate ($E_{\text{surface+adsorbate}}$) and the optimized clean surface with the adsorbing molecule optimized in the gas state ($E_{\text{surface}} + E_{\text{adsorbing molecule}}$),[39,40] as shown in the following equation:

$$E_{\text{ads}} = E_{\text{surface+adsorbate}} - (E_{\text{surface}} + E_{\text{adsorbing molecule}}) \quad (1)$$

Herein, taking into account the different pathways *via* the different intermediates mentioned above, we proposed two detailed mechanisms for the hydrogenation of CO_2 and CO on the Ru(0001) surface. The reaction mechanisms are schematically illustrated in Fig. 1. For CO_2 hydrogenation process, four possible pathways including CO_2 direct dissociation (Path I), decompositions *via trans*-COOH (Path II), *cis*-COOH (Path III) and an HCOO intermediate (Path IV) were investigated (Fig. 1a). The corresponding final products are HCOOH and CO, respectively, in which the produced CO species subsequently undergoes the hydrogenation pathways, as discussed in Fig. 1b. Three feasible reaction pathways of CO hydrogenation (CO + H) are investigated, including the C–O direct breaking (Path V) and the association of an H atom to form a COH or CHO intermediate (Path VI and Path VII, respectively). CH_4 and C_2 ($C_2H_xO_y$ compounds) are the corresponding final products. Herein, the reaction selectivity towards C_1 (C, CH, CH_2, CH_3, CH_4, CHOH and CH_2OH) and C_2 (CH_x–CH_y and CH_x–CO, x, y = 1, 2, 3) intermediates are discussed using kinetic analysis. The reaction energy of each pathway was calculated by the energy difference

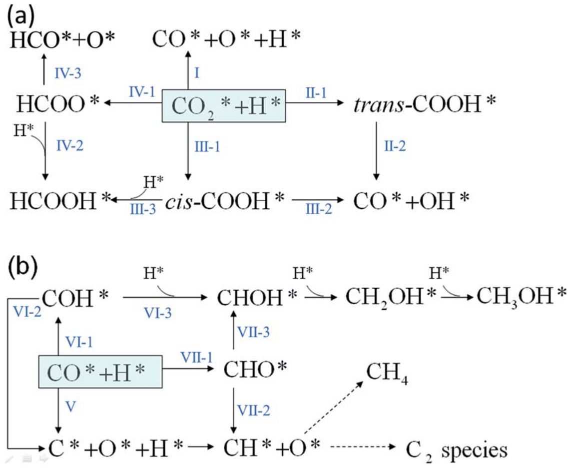

Fig. 1 Reaction mechanisms of the hydrogenation of (a) CO_2 and (b) CO.

between the product and the initial reactant of this pathway. The forward and reverse activation barriers of each reaction pathway are defined as the energy differences between the initial state and the saddle point, and between the saddle point and the final state, respectively.

3. Results and discussion

3.1 Adsorption of reactants and possible intermediates

To investigate the stability and configurations of the adsorbed species involved in the hydrogenation of CO_2 or CO on the Ru(0001) surface (Fig. 1), structural parameters and adsorption energies at their favorable sites are summarized in Table 1. The dissociated H atoms from H_2 are adsorbed at fcc sites with an adsorption energy of −3.15 eV (with respect to the H atom) and a Ru–H bond length of 1.88 Å. CO_2 weakly binds at the hcp site *via* a Ru–C bond (2.10 Å) with an adsorption energy of −0.52 eV. The bond angle $\angle$OCO changes from 180° in the gas state to 125.3° in the binding state, and the C atom forms three Ru–C bonds with adjacent metal atoms in an η^3 fashion, indicating that the CO_2 molecule is activated. CO prefers to non-dissociatively bind in the upright position with the C atom facing the top site on the Ru(0001) surface, whose adsorption energy (−2.30 eV) is significantly lower than that of CO_2. This value is slightly lower than the reported values (−1.87 ∼ −1.95 eV).[41,42] The C–O bond length in adsorbed CO is 1.16 Å and the Ru–C bond is 1.88 Å, which also agrees well with reported lengths (1.17 Å for C–O bonds, and 1.90 Å for Ru–C).

The key intermediate COOH is adsorbed at the Ru(0001) surface in two distinguishable configurations, *i.e.*, *trans*-COOH and *cis*-COOH, depending upon the direction of the hydroxyl group. The *cis*-COOH prefers to adsorb at the bridge site with an adsorption energy of −2.24 eV; while the *trans*-COOH is prone to adsorb at the fcc site with a slightly lower adsorption energy (−2.95 eV). When H atom binds at the C-end of CO_2 to form HCOO, the adsorption energy of HCOO decreases to −3.03 eV. CO_2 is weakly adsorbed, while the adsorption of the produced COOH and HCOO is significantly stronger. The rehybridization of the C atom in CO_2 after the association of H and CO_2 may induce the formation of σ bonds between the C atom in CO_2 and the adjacent metal atom, enhancing the adsorption of COOH and HCOO on the Ru(0001) surface.

The intermediate CHO tends to bind at the bridge site in a $\eta^1\eta^1$(C,O) manner, and the bond lengths of Ru–C and Ru–O are 1.98 and 2.17 Å, respectively. The calculated adsorption energy is −2.46 eV, agreeing with the previously reported results (−2.58 ∼ −2.62 eV).[43] For the COH species, it binds at the hcp site *via* Ru–C bonds (2.03 Å) in a η^3 mode, resulting in a considerably lower adsorption energy (−4.69 eV) in comparison with CHO. The C and CHCH intermediates are the C_1 and C_2 species, respectively, with the lowest adsorption energy. Being the final products of CO_2 and CO hydrogenation, HCOOH, CH_3OH, CH_4 and CH_3CH_3 interact weakly with the Ru(0001) surface with an adsorption energy of −0.78, −0.78, −0.17 and −0.34 eV, respectively, indicating that these products can easily escape from the Ru(0001) surface.

3.2 Dissociation and hydrogenation of CO_2

As discussed above, whether the hydrogenation of CO_2 starts from C–O bond breaking or from the association of hydrogen is still under debate. To elucidate this point, four possible reaction pathways for CO_2 hydrogenation are proposed (Fig. 1a), and the reaction barrier (E_a) along with the reaction energy (ΔE) of each elementary step are shown in Fig. 2. It can be seen that the direct dissociation of CO_2 (Path I: $CO_2^* \rightarrow CO^* + O^*$) is highly exothermic by −0.92 eV, indicating that this elementary step is thermodynamically favorable. However, its activation energy is relatively high (1.20 eV), suggesting the reaction does not easily occur. The corresponding configuration of the transition state is displayed in Fig. S1 (ESI†), in which the cleaving C–O bond is 1.62 Å. As listed in Table 1, CO and O species prefer to adsorb at the top site and the hcp site on the Ru surface, respectively, but in the transition state, both of them move to the fcc site and share a metal atom to form η^1-C–Ru and η^1-O–Ru bonds. These changes may lead to a high dissociation barrier of CO_2 direct dissociation.

The adsorbed COOH exists in two isomeric configurations, *trans*- and *cis*-COOH. The hydroxyl group in the *trans*-COOH points toward the Ru surface; while in the *cis*-COOH state, it points upwards and away from the surface. The calculated energy barrier for $CO_2^* + H^* \rightarrow$ *trans*-COOH*(Step II-1) is 1.04 eV and the reaction energy is −0.21 eV, indicating the CO_2 hydrogenation to *trans*-COOH is not feasible. The bond length of the produced O–H in the transition state (Fig. S2, ESI†) is 1.44 Å, accompanied with the co-adsorbed atomic H and CO_2 molecules moving towards each other. In the case of *cis*-COOH, the reaction energy and the energy barrier increases to 0.15 eV and 1.12 eV, respectively. The formed HCOO *via* Step IV-1 ($CO_2^* + H^* \rightarrow HCOO^*$) binds at the hcp site in a $\eta^1\eta^1\eta^1$(O,O,H) mode. At the transition state during HCOO formation, the surface atomic H moves from the hcp site towards the carbon atom, while the adsorbed CO_2 molecule does not move. As a result, the calculated energy barrier (0.37 eV) is lower than that of the CO_2 hydrogenation *via* the COOH intermediate. However, the energy barrier for the reverse reaction of Step IV-1 ($HCOO^* \rightarrow H^* + CO_2^*$, $E_a = 0.58$ eV) is significantly lower compared with the forward reaction (Step IV-2, $E_a = 1.13$ eV), indicating that the produced HCOO does not prefer to form HCOOH. The dissociation of HCOO to HCO and O (Step IV-3) was studied, and it was observed that this process is exothermic by 0.47 eV and requires an energy barrier of only 0.41 eV, indicating that this step, along with its previous reaction (Step IV-1), is the most energetically favorable pathway for the initial hydrogenation of CO_2.

By breaking the OC–OH bond, the *trans*- and *cis*-COOH decomposes into CO and OH. For the reaction of *trans*-COOH* → CO* + OH* (Step II-2), the reaction energy is −0.75 eV with an energy barrier of 1.48 eV, indicating that this step is only thermodynamically favorable. For the dissociation of *cis*-COOH (Step III-2), the activation barrier and the reaction energy are 0.09 eV and −1.11 eV, respectively, which are considerably lower than those of the pathway *via trans*-COOH, indicating a more favorable dissociation of *cis*-COOH into CO and OH. In the

Table 1 Optimized geometric parameters and adsorption energies (E_{ads}) of the species involved in CO_2/CO hydrogenation on the Ru(0001) surface

Adsorbate	E_{ads} (eV)	Site	d(Ru–A) (Å)		Bond length (Å) and bond angle (°) of adsorbed species			
H	−3.15	fcc	Ru–H	1.88				
CO_2	−0.52	hcp	Ru–C	2.10	d(C–O)	1.29	∠O–C–O	125.3
			Ru–O	2.15				
CO	−2.30	Top	Ru–C	1.88	d(C–O)	1.16		
cis-COOH	−2.24	hcp	Ru–C	2.02	d(O–H)	0.98	∠O–C–O	115.0
			Ru–O	2.18	d(C–O)	1.30	∠C–O–H	107.2
trans-COOH	−2.95	Bri	Ru–C	2.04	d(O–H)	0.99	∠O–C–O	114.6
			Ru–O	2.24	d(C–O)	1.34	∠C–O–H	106.7
HCOO	−3.03	hcp	Ru–C	2.54	d(C–H)	1.12	∠O–C–O	124.7
			Ru–O	2.11	d(C–O)	1.29	∠O–C–H	117.2
			Ru–H	2.43				
HCOOH	−0.78	hcp	Ru–C	2.14	d(C–H)	1.10	∠O–C–O	109.6
			Ru–O	2.13	d(C–O)	1.45	∠O–C–H	110.5
			Ru–H	2.70	d(O–H)	0.98	∠C–O–H	104.4
OH	−3.29	Bri	Ru–O	2.20	d(O–H)	0.97		
O	−2.86	hcp	Ru–O	2.01				
CHO	−2.46	Bri	Ru–C	1.98	d(C–O)	1.27	∠H–C–O	115.1
			Ru–O	2.17	d(C–H)	1.11		
COH	−4.69	hcp	Ru–C	2.03	d(C–O)	1.35	∠C–O–H	108.6
					d(O–H)	0.98		
CHOH	−3.92	hcp	Ru–C	2.04	d(C–O)	1.48	∠C–O–H	107.3
			Ru–O	2.24	d(C–H)	1.10	∠O–C–H	107.2
			Ru–H	3.16	d(O–H)	0.98		
CH_2OH	−2.48	fcc	Ru–C	2.13	d(C–O)	1.48	∠C–O–H	105.2
			Ru–O	2.30	d(C–H)	1.12	∠H–C–H	101.7
			Ru–H	1.96	d(O–H)	0.98		
CH_3OH	−0.78	Bri	Ru–C	3.25	d(C–O)	1.45	∠C–O–H	109.1
			Ru–O	2.30	d(C–H)	1.10		
			Ru–H	2.93	d(O–H)	0.98		
C	−7.76	hcp	Ru–C	1.93				
CH	−7.28	hcp	Ru–C	2.02	d(C–H)	1.10		
CH_2	−4.86	hcp	Ru–C	2.13	d(C–H)	1.12	∠H–C–H	105.1
CH_3	−2.62	hcp	Ru–C	2.28	d(C–H)	1.12	∠H–C–H	106.2
CH_4	−0.17	Top	Ru–C	3.31	d(C–H)	1.11	∠H–C–H	107.7
CH_3CO	−3.03	Bri	Ru–C_{down}	1.99	d(C–H)	1.10	∠H–C–H	107.7
			Ru–C_{up}	3.09	d(C–C)	1.50	∠C–C–O	102.4
					d(C–O)	1.28		
CH_3CH	−4.97	fcc	Ru–C_{down}	2.08	d(C–H)	1.20	∠C–C–H	99.6
					d(C–C)	1.51		
CH_3CH_2	−2.10	Bri	Ru–C_{down}	2.14	d(C–H)	2.14		
					d(C–C)	1.53		
CHCH	−6.62	Bri	Ru–C_{down}	2.15	d(C–H)	1.10		
					d(C–C)	1.43		
$CHCH_2$	−3.82	fcc	Ru–C_{down}	2.03	d(C–H)	1.09		
					d(C–C)	1.43		
CH_2CH_2	−1.52	Top	Ru–C_{down}	2.15	d(C–H)	1.11		
					d(C–C)	1.45		
CHCO	−4.13	Bri	Ru–C_{down}	2.15	d(C–H)	1.09		
					d(C–C)	1.41		
CH_2CO	−2.16	fcc	Ru–C_{down}	2.07	d(C–H)	1.09		
					d(C–C)	1.44		
CH_3CH_3	−0.34	fcc	Ru–C	4.05	d(C–H)	1.10		
					d(C–C)	1.52		

transition state of this step, the co-adsorbed CO and OH attain at the stable top and fcc sites without sharing metal atoms, resulting in a rather low *cis*-COOH dissociation barrier. Alternative pathways involves hydrogenation at the C-end of *cis*-COOH to form the HCOOH intermediate (Step III-3, Fig. 2) but a high activation barrier (0.88 eV) and reaction energy (0.80 eV) excludes the unfavorable elementary step: *cis*-COOH* + H* → HCOOH*. The total change in energy along Path III and Path IV is not the same (Fig. 2), which is mainly because the energy change in the co-adsorption process of H and COOH is different from that in the co-adsorption process of H and *cis*-COOH (Fig. S5†).

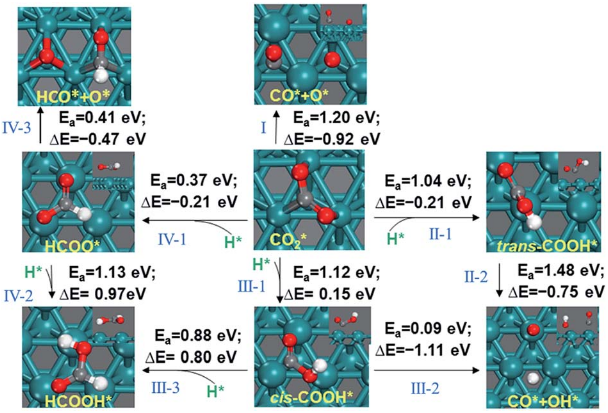

Fig. 2 Dissociation (Path I), hydrogenation of CO_2 (Step II-1, Step III-1 and Step IV-1), dissociation of carboxyl (Step II-2 and Step III-2), formation of formic acid on the Ru(0001) surface (Step III-3 and Step IV-4), denoted with their energy barriers (E_a) and reaction energies (ΔE). Cyan, Ru; red, O; white, H; gray, C.

The energy profiles of the four reaction pathways of CO_2 dissociation are summarized in Fig. 3. The results demonstrate that the overall barrier along Path IV (*via* the HCOO to CHO intermediate) is significantly lower than that along the *trans*-COOH pathway (Path II) or *via* the *cis*-COOH intermediate to CO or HCOOH (path III); the direct CO_2 dissociation on the Ru(0001) surface (Path I) shows a much higher overall barrier (1.20 eV). According to the Arrhenius formula, the calculated rate of CO_2 hydrogenation to HCOO (Step IV-1) is 4.0×10^5 to 2.0×10^6 times larger than the COOH formation rate at a temperature of 600 K. Therefore, the CO_2 hydrogenation to HCOO (Step IV-1) is more favorable than the *cis*- and *trans*-COOH intermediate (Path II and III). The further hydrogenation of HCOO to HCOOH (Step IV-2) has an energy barrier of 1.13 eV, which is significantly higher than that of HCOOH dissociation back to HCOO and H by 0.97 eV. Therefore, it is expected that the HCOOH formed would quickly dissociate back to HCOO and atomic H. The dissociation pathway of HCOO to CHO and O was also investigated, and the highest individual barrier along this route was only 0.41 eV (at Step IV-3) with relatively low energy trace. As a result, it is concluded that adsorbed CO_2 on the Ru(0001) surface prefers to first undergo hydrogenation to HCOO, and sequentially dissociates to CHO and O; while the dissociation *via* COOH intermediate is not favorable. This agrees well with the experimental observations that abundant HCOO was observed instead of COOH intermediate.[44] In general, it is believed that CO_2 first converts to CO on Ru catalysts, followed by CO hydrogenation to methane.[21] In addition, the process of the dissociation of CHO to CO and H was also studied in this work, and the results showed that CO intermediate mainly arises from the direct dissociation of CHO, which is the reverse reaction of CO hydrogenation. More details will be disclosed in the following section.

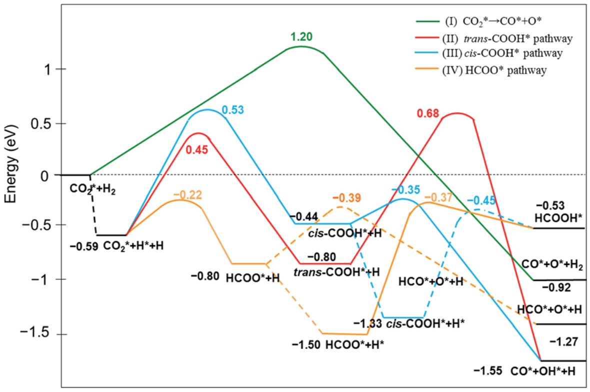

Fig. 3 Energy profiles for CO_2 dissociation and hydrogenation, dissociation of carboxyl, and the formation of formic acid on the Ru(0001) surface. The energy sum of the adsorbed CO_2 and H_2 is set as zero.

3.3 CO hydrogenation

In the case of CO hydrogenation, three possible reaction routes were considered (Path V, VI and VII, Fig. 4). Our calculations show that the direct dissociation of CO (Path V: $CO^* \rightarrow C^* + O^*$) is endothermic with the reaction energy as high as 1.08 eV and energy barrier of 2.63 eV (Fig. 4). CO is prone to independently adsorb on the top site, where the C atom adopts an sp hybridization to form σ-Ru–C bond with a very short length (1.88 Å, Table 1). At the transition state, the C and O atom move to the hcp and fcc site, respectively, and the distance between C and O is 1.81 Å. The high dissociation barrier of Path V is possibly attributed to the high energy required for the breaking of the Ru–C bond. When co-adsorbed with H atom, CO tends to bind at the bridge site, while the H atom is at the hcp site (Fig. S7, ESI†); the hydrogenation towards an COH intermediate (Step VI-1) is endothermic by 1.24 eV with an energy barrier of 1.69 eV. Step VII-1 involves hydrogenation at the C-end of CO to form a CHO intermediate (Fig. 4) with an activation barrier of 1.29 eV and the reaction energy of 0.93 eV, which is significantly lower than the values *via* the COH intermediate (Step VI-1). In addition, CO dissociation from the COH and CHO intermediate was also investigated (Fig. 4), whose barriers are 0.71 eV (Step VI-2) and 1.02 eV (Step VII-2), respectively. This implies that the C–OH bond breaks more easily on the Ru(0001) surface compared with the HC–O bond. The calculated barriers and

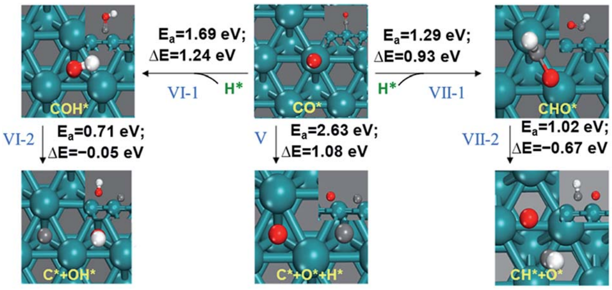

Fig. 4 Dissociation (Path V) and hydrogenation of CO (Path VI and VII), dissociation of COH and CHO on the Ru(0001) surface (cyan, Ru; red, O; white, H; gray, C), denoted with their reaction barriers (E_a) and reaction energies (ΔE).

reaction energies in this work agree well with the DFT study reported by Inderwildi *et al.* regarding CO dissociation *via* path V and path VII.[26]

3.4 Formation of CH_3OH

Because both COH and CHO could be further hydrogenated to CHOH,[2] the reaction pathways involving the formation of CH_3OH from COH and CHO (Step VI-3 and VII-3, Fig. 5) were investigated. The formation barrier from co-adsorbed CHO and H to CHOH is 1.24 eV with a reaction energy of 0.62 eV. The hydrogenation at the C-end of COH to form the CHOH intermediate is also endothermic with an energy barrier of 0.96 eV, which is higher than the direct dissociation of COH (Step VI-2) by 0.25 eV. This suggests that the hydrogenation reactions of both CHO and COH intermediate to CHOH are unfavorable. CH_2OH can be produced by the hydrogenation of CHOH, which is found to be endothermic (0.36 eV) with an energy barrier of 0.66 eV; further endothermic (0.31 eV) hydrogenation of CH_2OH to CH_3OH requires an energy barrier of 0.93 eV. The sequence of hydrogenations to CH_3OH with an endothermic property and high barriers imply that the reactions toward alcohol may not occur.

The energy profiles of CO dissociation and hydrogenation are summarized in Fig. 6. Our results show that direct CO dissociation on the Ru(0001) surface (Path V) requires an energy barrier as high as 2.63 eV; while CO dissociation barriers *via* the COH intermediate (Step VI-1 and VI-2) and *via* the CHO intermediate (Step VII-1 and Step VII-2) are equal (1.95 eV, Fig. 6). In this case, CO dissociation is more favorable *via* CHO or COH than the direct dissociation (Path V), not only because of the lower barrier of the former pathway, but also because of a higher stability of the produced intermediates. The COH and CHO intermediates kinetically prefer to directly dissociate rather than associate with H to form CHOH species (pink and green dashes in Fig. 6)due to the lower barrier of the dissociation pathway. In fact, each step of the CH_3OH formation from CHOH and H atom is endothermic, while the dissociation steps of COH and CHO are exothermic (Fig. 5). Therefore, rather than the CH_3OH formation, CO hydrogenation may be prone to produce C and CH intermediate on the Ru(0001). For CHO species produced by the CO_2 hydrogenation and subsequent dissociation (Fig. 3), the calculated results in Fig. 6 show that the dissociation of CHO to CO and H is exothermic by 0.93 eV with a barrier of 0.36 eV; while the forward CHO dissociation to CH and O should overcome an energy barrier as high as 1.02 eV. This suggests that the produced CHO species may hardly dissociate to CH and O until the dissociation of CHO to CO and H reaches an equilibrium state. This result explains why the required temperature for CO_2 hydrogenation is significantly lower compared with that for CO hydrogenation:[45] the reaction from CO_2 to CHO is entirely exothermic and the individual barrier for each step is low; while CO hydrogenation to CHO is endothermic with an energy barrier of 1.69 eV.

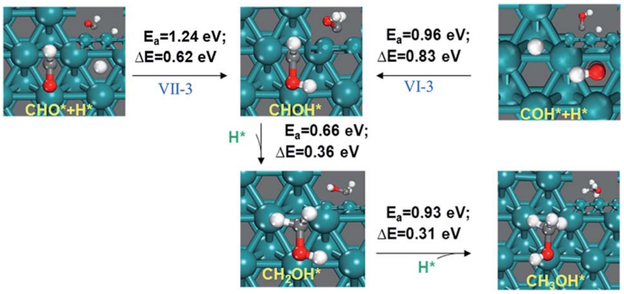

Fig. 5 Hydrogenation of COH, CHO, CHOH and CH_2OH on the Ru(0001) surface (cyan, Ru; red, O; white, H; gray, C), denoted with their reaction barriers (E_a) and reaction energies (ΔE).

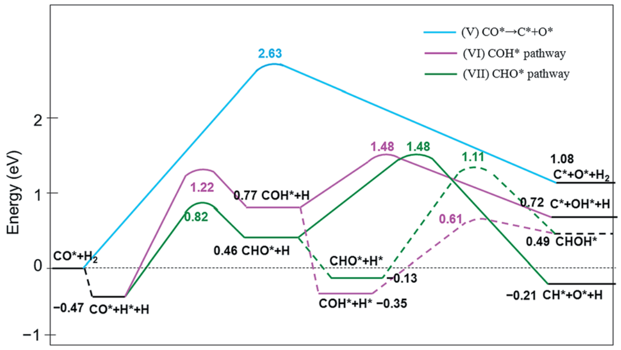

Fig. 6 Energy profiles for the dissociation and hydrogenation of CO, COH, CHO on the Ru(0001) surface, respectively. The energy sum of the adsorbed CO and H_2 is set as zero.

3.5 Formation of CH_x (x = 1–4)

CH formation. The geometries and energy pathways for the formation of CH_4 on the Ru(0001) surface are presented in Fig. 7. During the initial state of the formation of CH, C and H atoms attach to the hcp and bridge site, respectively, with a distance of 2.79 Å. In the transition state, the distance of the C–H bond is 1.46 Å, which is very close to that of the adsorbed CH species (1.10 Å, Table 1), implying that CH formation from C and H possesses a late transition state. In the final state, the adsorbed CH species is located in an upright position with the C-end facing the hcp site. The barrier for CH formation is

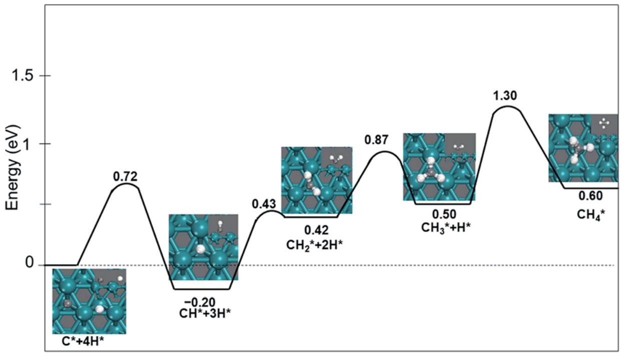

Fig. 7 Stepwise hydrogenations of carbon to CH, CH_2, CH_3 and CH_4 on the Ru(0001) surface (cyan, Ru; red, O; white, H; gray, C), denoted with reaction barriers (E_a) and reaction energies (ΔE).

0.72 eV, which is consistent with the previously reported DFT calculations (0.75 eV).[46]

CH_2 formation. CH_2 formation on the Ru(0001) surface is endothermic by 0.62 eV with an energy barrier of 0.63 eV. The dehydrogenation from CH_2 to CH requires only 0.01 eV, implying that CH_2 may easily dissociate back to CH and H. In the initial state, both the CH and H are co-adsorbed at the adjacent hcp sites with a distance of 2.76 Å. In the transition state, both the CH and H are located at the hcp site and the formed C–H bond length is 1.52 Å. In the final state, CH_2 also remains at the hcp site with a C–H bond length of 1.12 Å. The similar adsorption and configuration of HC–H in the transition state and in the final state demonstrate that the reaction exhibits a late transition state.

CH_3 and CH_4 formation. The hydrogenation of CH_2 is endothermic (0.08 eV) and requires an energy barrier of 0.45 eV. It has been reported that the CH_3 intermediate was stabilized at the bridge site on corrugated surfaces.[32] In contrast, we observed that CH_3 moves from the bridge site to the hcp site in a flat Ru(0001) surface during optimization. The hydrogenation of CH_3 is the final step in the formation of CH_4 and the reverse reaction is the initial step for CH_4 dissociation. In the transition state of CH_4 formation, the co-adsorbed CH_3 and H are separated by 1.52 Å. In this configuration, the CH_3 group moves towards the top site and shares it with the attacking H atom. In the final state, CH_4 moves over the top site and weakly interacts with the Ru(0001) surface.

The reaction pathway for the hydrogenation of C to methane along with the energy profiles are shown in Fig. 7. The formation of CH_4 from CH_3 and H requires the highest activation energy (0.93 eV), which is the rate-limiting step in the sequence of hydrogenation reactions of C to CH_4. van Santen *et al.* reported the overall barrier for the formation of CH_4 from active C and H on corrugated Ru(1010) surface is ~2.02 eV.[32] In this work, the overall barrier of CH_4 formation on flat Ru(0001) surface is 1.63 eV. This implies that compared with the corrugated Ru(1010) surface, the flat Ru(0001) surface is advantageous in catalyzing carbon hydrogenation to CH_4. The calculated reaction energy of CH_4 formation from CO_2 is −0.90 eV (the experimental value is −0.67 eV at 298 K)[15] with an overall barrier of 0.37 eV; while CO_2 hydrogenation to CH_3OH is endothermic by 0.26 eV and requires an overall barrier of 1.23 eV. For CO hydrogenation, CH_4 formation was calculated to be −1.07 eV (the experimental value is −2.10 eV at 298 K)[15] and overcomes an energy barrier of 1.95 eV (0.30 eV lower than CH_3OH formation). This demonstrates that CH_3OH is an unfavorable product of CO_2/CO hydrogenation on Ru(0001) surface.

3.6 C–C Coupling of chain growth reactions

The reaction pathways of all the possible C–C coupling reactions on the Ru(0001) surface among CO, CH, CH_2 and CH_3 were studied (Table 2). The results show that the lowest barrier channel of C–C coupling on flat Ru(0001) surface occurs *via* the CH + CH reaction with an energy barrier of 0.77 eV. In the initial state of CH + CH reaction, two methynes are co-adsorbed at the adjacent fcc sites *via* η^3-C–Ru mode. In the transition state, only two C–Ru bonds are broken, and one strong σ and two π bonds are formed between the two coupled carbon atoms (Fig. S15, ESI†). This may lead to the relatively low reaction barrier required for the CH + CH reaction. Moreover, the adsorption energy of the formed CHCH intermediate (−6.62 eV, Table 1) is much higher than that of the co-adsorbed CH intermediate (−13.67 eV) because of the formation of C–C bond. Note that all the C–C coupling reactions between CH_x and CO have a high barrier (Table 2), suggesting that carbon chain growth reactions hardly occur between CH_x species and CO. This is mainly attributed to the adsorption configuration (in a tilt mode) of CH_xCO species on the Ru(0001) surface, in which the OC-end is significantly closer to the surface than the H_xC-end. Therefore, C–C bond formation between CH_x species and CO should overcome the higher energy barrier.

Table 2 Calculated barriers and reaction energies of the C–C coupling reactions

Reaction	Reaction barrier (eV)	Heat of reaction (eV)
$CH^* + CO^* \rightarrow CHCO^*$	1.22	0.97
$CH^* + CH^* \rightarrow CHCH^*$	0.77	−0.35
$CH^* + CH_2^* \rightarrow CHCH_2^*$	1.30	0.24
$CH^* + CH_3^* \rightarrow CHCH_3^*$	1.08	−1.33
$CH_2^* + CO^* \rightarrow CH_2CO^*$	1.58	0.71
$CH_2^* + CH_2^* \rightarrow CH_2CH_2^*$	0.95	−0.22
$CH_2^* + CH_3^* \rightarrow CH_2CH_3^*$	0.85	−0.01
$CH_3^* + CO^* \rightarrow CH_3CO^*$	1.42	0.64
$CH_3^* + CH_3^* \rightarrow CH_3CH_3^*$	1.33	−0.03

According to our calculation, the CH_x + CO reactions (Table 2) have a high reaction barrier, suggesting that the Ru(0001) surface is beneficial for C–O bond cleavage other than alcohol production. Therefore, we calculated the reaction rates of two pathways derived from C–O bond cleavage, CH_i + H ($i = 0$, 1, 2, 3) and CH_i + CH_j ($i, j = 1, 2, 3$), by kinetic methods to analyze product selectivity (methane or liquid hydrocarbons) of CO_2 or CO hydrogenation on the Ru(0001) surface. The reaction rates of C chain growth, hydrogenation of CH and CH_4 formation reaction were evaluated (Table 3) using Cheng's method[47–49] according to the calculated energy barriers and reaction energies listed in Fig. 7 and Table 2 (the theory for kinetic analysis is described in the ESI†). Based on the results in Table 3, it can be clearly seen that all the C–C coupling reactions, except the CH + CH reaction, can be negligible due to their low reaction rates. The CH_2 + CH_3 and CH + CH reactions are the two reactions with the lowest barriers (Table 2), however, the former reaction is hardly reactive due to the low reaction rates of CH_2 and CH_3 formation (Table 3). Because of a direct competition against CH–CH coupling reaction, the CH hydrogenation is also favorable since the reaction rate of CH hydrogenation is rather high ($2.45 \times 10^9\ \theta_C t^2$, Table 3) with $r_{CH+CH}/r_{CH+H} = 3.19 \times \theta_C/\theta^*$. If θ_C is much less than θ^*, the CH + H reaction would be more favorable to produce CH_2; otherwise the CH + CH coupling reaction would be much faster to give C–C chain growth. The ratio of θ_C to θ^* is positively correlated to the CO_2/CO fraction and reaction pressure. Furthermore,

Table 3 Reaction rates (s^{-1}) of the stepwise carbon hydrogenation and C–C coupling reactions on the Ru(0001) surface[a]

Reaction pathway	Reaction rate
CH + CH	$7.82 \times 10^9\ \theta^2{}_\mathrm{C}t^2$
$CH + CH_2$	$1.73 \times 10^0\ \theta^2{}_\mathrm{C}t^3$
$CH + CH_3$	$2.59 \times 10\ \theta^2{}_\mathrm{C}t^4$
$CH_2 + CH_2$	$9.35 \times 10^{-3}\ \theta^2{}_\mathrm{C}t^4$
$CH_2 + CH_3$	$1.37 \times 10^{-2}\ \theta^2{}_\mathrm{C}t^5$
$CH_3 + CH_3$	$2.74 \times 10^{-7}\ \theta^2{}_\mathrm{C}t^6$
CH hydrogenation	$2.45 \times 10^9\ \theta_\mathrm{C}t^2$
CH_4 formation	$1.25 \times 10^2\ \theta_\mathrm{C}t^4$

[a] The selected temperature is 600 K, which is in line with the work previously reported.[31]

considering the temperature effect (T), $r_{\mathrm{CH+CH}}/r_{\mathrm{CH+H}}$ equals $\exp(-0.57\ \mathrm{eV}/RT)\theta_\mathrm{C}/\theta^*$, indicating that a high temperature promotes the C–C coupling reaction over methanation. These results are consistent with the experimental observations: Ru selectively produces methane at normal pressure with a relatively high H_2 fraction, while long-chain hydrocarbons are the predominant products at high pressure with moderate H_2 content. The F–T reactions usually require a higher temperature than methanation reactions.[50–56]

4. Conclusions

DFT calculations were carried out to investigate the hydrogenation process of CO_2 and CO on the Ru(0001) surface, respectively, including the adsorption of possible intermediates, reaction mechanism and factors determining the product selectivity. For CO_2 hydrogenation, the adsorbed CO_2 first undergoes hydrogenation to a HCOO intermediate and produces an adsorbed CHO and O species. In the case of CO hydrogenation, it is found that CO may dissociate *via* either a COH or CHO intermediate, resulting in C and CH species, respectively. The active C and CH species then undergo stepwise hydrogenation to CH_2, CH_3 and CH_4, or the CH_x species further transforms to longer carbon chains. Calculations reveal that CH_3 hydrogenation is the rate-determining step in the sequence of C hydrogenation on the Ru(0001) surface, and the lowest barrier channel of C–C coupling occurs *via* the CH + CH reaction. The reaction rates of CH + H and $CH_i + CH_j$ ($i, j = 1, 2, 3$) were obtained by kinetic methods in an effort to reveal the selectivity of the final products. The results show that methane will dominate the final product with a high H_2 fraction in the reaction at normal reaction pressure, while the chain growth reactions are more favorable with a high CO or CO_2 fraction at relatively high pressures. This theoretical work provides a fundamental insight into the reaction mechanism of CO_2 and CO hydrogenation on the Ru(0001) surface, which is useful for the exploration of noble-metal catalysts and recycling of carbon resources.

Acknowledgements

This work was supported by the 973 Program (Grant no.: 2011CBA00504), the National Natural Science Foundation of China (NSFC), the Scientific Fund from Beijing Municipal Commission of Education (20111001002) and the Fundamental Research Funds for the Central Universities (ZD 1303). The "Chemical Grid Project" of Beijing University of Chemical Technology is appreciated. M. Wei particularly appreciates the financial aid from the China National Funds for Distinguished Young Scientists of the NSFC.

Notes and references

1 H. J. Smith, J. Fahrenkamp-Uppenbrink and R. Coontz, *Science*, 2009, **325**, 1641.
2 Y. F. Zhao, Y. Yang, C. Mims, C. H. F. Peden, J. Li and D. Mei, *J. Catal.*, 2011, **281**, 199.
3 O. O. James, B. Chowdhury, M. A. Mesubi and S. Maity, *RSC Adv.*, 2012, **2**, 7347.
4 S. Park, D. Bezier and M. Brookhart, *J. Am. Chem. Soc.*, 2012, **134**, 11404.
5 W. Wang, S. P. Wang, X. P. Ma and J. L. Gong, *Chem. Soc. Rev.*, 2011, **40**, 3703.
6 S. Sharma, Z. P. Hua, P. Zhang, E. W. McFarland and H. Metiu, *J. Catal.*, 2011, **278**, 297.
7 A. Y. Khodakov, W. Chu and P. Fongarland, *Chem. Rev.*, 2007, **107**, 1692.
8 N. Perkas, J. Teo, S. Shen, Z. Wang, J. Highfield, Z. Zhong and A. Gedanken, *Phys. Chem. Chem. Phys.*, 2011, **13**, 15690.
9 G. A. Morgan, D. C. Sorescu, T. Zubkov and J. T. Yates, *J. Phys. Chem. B*, 2004, **108**, 3614.
10 Z. Z. Yang, Y. N. Zhao and L. N. He, *RSC Adv.*, 2011, **1**, 545.
11 A. Karelovic and P. Ruiz, *Appl. Catal., B*, 2012, **113**, 237.
12 D. Tang and J. Zhang, *RSC Adv.*, 2013, **3**, 15225.
13 A. X. Yin, W. C. Liu, J. Ke, W. Zhu, J. Gu, Y. W. Zhang and C. H. Yan, *J. Am. Chem. Soc.*, 2012, **134**, 20479.
14 V. M. Shinde and G. Madras, *RSC Adv.*, 2014, **4**, 4817.
15 P. Panagiotopoulou, D. I. Kondarides and X. E. Verykios, *J. Phys. Chem. C*, 2011, **115**, 1220.
16 M. R. Prairie, A. Renken, J. G. Highfield, K. P. Thampi and M. Grätzel, *J. Catal.*, 1991, **129**, 130.
17 H. Y. Kim, H. M. Lee and J. N. Park, *J. Phys. Chem. C*, 2010, **114**, 7128.
18 H. Yoshida, S. Narisawa, S. Fujita, L. Ruixia and M. Arai, *Phys. Chem. Chem. Phys.*, 2012, **14**, 4724.
19 M. P. Andersson, F. Abild-Pedersen, I. N. Remediakis, T. Bligaard, G. Jones, J. Engbæk, O. Lytken, S. Horch, J. H. Nielsen, J. Sehested, J. R. Rostrup-Nielsen, J. K. Nørskov and I. Chorkendorff, *J. Catal.*, 2008, **255**, 6.
20 O. R. Inderwildi, S. J. Jenkins and D. A. King, *J. Phys. Chem. C*, 2008, **112**, 1305.
21 S. Eckle, H. G. Anfang and R. J. Behm, *J. Phys. Chem. C*, 2011, **115**, 1361.
22 J. N. Park and E. W. McFarland, *J. Catal.*, 2009, **266**, 92.
23 L. F. Liotta, G. A. Martin and G. Deganello, *J. Catal.*, 1996, **164**, 322.
24 E. Vesselli, M. Rizzi, L. D. Rogatis, X. L. Ding, A. Baraldi, G. Comelli, L. Savio, L. Vattuone, M. Rocca, P. Fornasiero, A. Baldereschi and M. Peressi, *J. Phys. Chem. Lett.*, 2010, **1**, 402.

25 W. J. Mitchell, Y. Wang, J. Xie and W. H. Weinberg, *J. Am. Chem. Soc.*, 1993, **115**, 4381.

26 O. R. Inderwildi, S. J. Jenkins and D. A. King, *Angew. Chem., Int. Ed.*, 2008, **47**, 5253.

27 D. W. Goodman, R. D. Kelley, T. E. Madey and J. T. Yates, *J. Catal.*, 1980, **63**, 226.

28 H. P. Bonzel and H. J. Krebs, *Surf. Sci.*, 1980, **91**, 499.

29 N. M. Gupta, V. P. Londhe and V. S. Kamble, *J. Catal.*, 1997, **169**, 423.

30 S. Shetty, A. P. J. Jansen and R. A. van Santen, *J. Am. Chem. Soc.*, 2009, **131**, 12874.

31 J. Chen and Z. P. Liu, *J. Am. Chem. Soc.*, 2007, **130**, 7929.

32 S. Shetty, A. P. J. Jansen and R. A. van Santen, *J. Phys. Chem. C*, 2010, **114**, 22630.

33 I. M. Ciobica, F. Frechard, R. A. van Santen, A. W. Kleyn and J. Hafner, *J. Phys. Chem. B*, 2000, **104**, 3364.

34 J. W. Mirwald and O. R. Inderwildi, *Phys. Chem. Chem. Phys.*, 2012, **14**, 7028.

35 B. Delley, *J. Chem. Phys.*, 1990, **92**, 508.

36 B. Delley, *J. Chem. Phys.*, 1996, **100**, 6107.

37 B. Delley, *J. Chem. Phys.*, 2000, **113**, 7756.

38 J. P. Perdew, J. A. Chevary, S. H. Vosko, K. A. Jackson, M. R. Pederson, D. J. Singh and C. Fiolhais, *Phys. Rev. B: Condens. Matter Mater. Phys.*, 1992, **46**, 6671.

39 I. D. Rosal, L. Truflandier, R. Poteau and I. C. Gerber, *J. Phys. Chem. C*, 2011, **115**, 2169.

40 I. D. Rosal, T. Gutmann, B. Walaszek, I. C. Gerber, B. Chaudret, H. H. Limbach, G. Buntkowsky and R. Poteau, *Phys. Chem. Chem. Phys.*, 2012, **113**, 20199.

41 R. A. Olsen, G. J. Kroes, G. Henkelman, A. Arnaldsson and H. Jonsson, *J. Chem. Phys.*, 2004, **121**, 9776.

42 G. Henkelman and H. Jonsson, *J. Chem. Phys.*, 2000, **113**, 9978.

43 I. M. Ciobica and R. A. van Santen, *J. Phys. Chem. B*, 2003, **107**, 3808.

44 Y. Yang, C. A. Mims, R. S. Disselkamp, D. Mei, J. H. Kwak, J. Szanyi, C. H. F. Penden and C. T. Campbell, *Catal. Lett.*, 2008, **125**, 201.

45 N. M. Gupta, V. S. Kamble, V. B. Kartha, R. M. Iyer, K. Ravindranathan Thampi and M. Gratzel, *J. Catal.*, 1994, **146**, 173.

46 I. M. Ciobica and R. A. van Santen, *J. Phys. Chem. B*, 2002, **106**, 6200.

47 J. Cheng, P. Hu, P. Ellis, S. French, G. Kelly and C. M. Lok, *J. Phys. Chem. C*, 2009, **113**, 8858.

48 J. Cheng, X. Q. Gong, P. Hu, C. M. Lok, P. Ellis and S. French, *J. Catal.*, 2008, **254**, 285.

49 J. Cheng, P. Hu, P. Ellis, S. French, G. Kelly and C. M. Lok, *J. Phys. Chem. C*, 2010, **114**, 1085.

50 H. Schulz, *Appl. Catal., A*, 1999, **186**, 3.

51 O. R. Inderwildi, S. J. Jenkins and D. A. King, *J. Phys. Chem. C*, 2008, **112**, 1305.

52 G. A. Mills and F. W. Steffgen, *Catal. Rev.: Sci. Eng.*, 1974, **8**, 159.

53 Y. Traa and J. Weitkamp, *Chem. Eng. Technol.*, 1999, **21**, 291.

54 W. Wang and J. Gong, *Front. Chem. Sci. Eng.*, 2011, **5**, 2.

55 A. P. Steynberg, R. L. Espinoza, B. Jager and A. C. Vosloo, *Appl. Catal., A*, 1999, **186**, 41.

56 T. Abe, M. tanzawa, K. Watanabe and A. Taguchi, *Energy Environ. Sci.*, 2009, **2**, 315.